AERODYNAMIC DESIGN OF A FORMULA SAE RACE CAR

Andrew R. Hammond[*] and Richard G.J. Flay[†]

[*] Former Masters Student, Department of Mechanical Engineering
The University of Auckland, Private Bag 92019, Auckland, New Zealand
e-mail: `andrew_r_hammond@hotmail.com`,

[†] Professor, Department of Mechanical Engineering
The University of Auckland, Private Bag 92019, Auckland, New Zealand
e-mail: `r.flay@auckland.ac.nz`

Keywords: Formula SAE, rolling road, vehicle aerodynamics, wind tunnel test, race-car.

Abstract. *The objective of the research in this paper was to maximise the amount of performance enhancing aerodynamic down-force generated by the 2005/2006 University of Auckland Formula SAE race car. This was done through a combination of physical modelling using a rolling road wind tunnel research facility and by using computational fluid dynamics.*

Computational fluid dynamic analysis was used for the design of the body and under-tray of the vehicle. Optimal design gave a lift coefficient of -0.9 from the under-tray. Simulations showed that when the exhaust was vented into two diffuser tunnels under the car, the down-force was increased by 35%. Half-scale vehicle modelling using the wind tunnel rolling road facility gave a lift coefficient of -2.4. In its optimal configuration, the aerodynamic load on the front and rear wheels respectively was able to be adjusted between 43% on the front and 57% on the rear to 33% on the front and 67 % on the rear by changing the angle of the foils. The drag coefficient varied from 0.9 to 1.1.

Full-scale on-track measurements showed that only 6% less down-force was being generated than was predicted from the wind tunnel test programme, and validated the experimental approach that was taken. Data collected from the car during the endurance event at the 2006 Formula Student Germany competition showed that the aerodynamic package was responsible for a significant increase in the performance of the vehicle under braking and during cornering, while the increase in the drag force had only a minimal effect on the top speed which was achieved during the event.

1   INTRODUCTION

1.1   The nature of the problem

Aerodynamic down-force is hugely exploited in the design of the modern race car, Refs [1,2]. The performance benefits which can be gained through the resulting increase in traction has made the search for increased down-force and reduced drag a highly sought after performance edge in motor sport. The benefits of an effective aerodynamic design in the Formula SAE competition is still, however, a topic of debate. It was the goal of the present research to determine areas where the aerodynamic forces are most performance enhancing by utilising CFD as well as model testing in a wind tunnel equipped with a moving belt ground plane, and then to validate the predictions using on-road measurements from the 2005/2006 University of Auckland Formula SAE race car. Further details are available in Ref. [3].

1.2   The Formula SAE Competition

The Formula SAE competition was established in 1981 by the Society of Automotive Engineers (SAE) in the United States of America as an educational tool to develop the knowledge and skill base of the automotive industry at the university level. The competition requires that each team from their respective universities design, build, and test a small, open-wheeled, single-seater race-car with the premise that a manufacturing firm has employed the team to design the vehicle for a one-make racing series, for which the cost to reproduce each of the vehicles must not exceed US$25,000. The competition comprises both static and dynamic events. The static events consist of a business and design presentation each of which are marked by a panel of experts. A tilt test of the vehicle is also performed to simulate cornering and to determine the height of the centre of gravity of the vehicle. The dynamic events aim to test the vehicle in all aspects of competition car performance with acceleration, skid pan cornering, autocross, and a final 22 km endurance test. Marks are awarded for the performance of the vehicle in each of these tests as well as on the fuel economy of the vehicle during the endurance event. The total marks received from both the static and the dynamic events determine the overall winner of the competition.

1.3   The Influence of aerodynamics on race car performance

The fundamental goal of any race car design is to *"….provide the driver the means to control and change the velocity of the vehicle at the greatest rate possible – acceleration. Their vehicle is the system by which artificial forces (i.e, non-human forces) are generated in order to accelerate the driver's body while he attempts to use the vehicle control systems to maintain the highest possible acceleration level, in the appropriate direction, at all times. For maximum acceleration, the force generation systems must be as powerful as possible and their mass, added to that of the driver and including the fuel necessary, as small as possible."* which is quoted from Peter Wright, former Technical Director of Team Lotus, Ref.[4].

The resultant forces which occur during the operation of a road vehicle during its operation can be split into three categories: (i) acceleration, (ii) cornering and (iii) braking (deceleration). Each of these must be transferred to the surface on which the vehicle is travelling in order for the driver to be in control of the vehicle. This transfer of these forces is via the tyres' contact surfaces.

It is useful to analyse the force at the tyre/road surface interface to see what influences it. The maximum horizontal force which can be achieved between a tyre and the road surface is dependent on the normal force at the interface and the friction coefficient, μ_{max} , Ref. [4]

$$F_{horizontal} = F_{vertical} \times \mu_{max} \tag{1}$$

where
$$F_{vertical} = M \times g \tag{2}$$

and M is mass. Thus a greater normal force placed on the tyre will increase the available traction and apparently increase the subsequent performance of the vehicle given a constant coefficient of friction, and can be done simply by increasing the mass of the vehicle. However, this contravenes Peter Wright's fundamental goal given at the beginning of this section. The horizontal acceleration is given by

$$Acceleration = \frac{F_{horizontal}}{M} = \frac{M \times g \times \mu_{max}}{M} = g \times \mu_{max} \tag{3}$$

and hence the maximum horizontal acceleration of a vehicle is independent of its mass.

Consequently it is clearly desirable to increase the downward force on the tyres without increasing the mass of the vehicle, and this is where aerodynamic down-force is extremely important. With the addition of aerodynamic down-force the vertical force equation becomes:

$$F_{vertical} = [M \times g] + \text{down-force} , \tag{4}$$

and the maximum acceleration which is now achievable is:

$$Acceleration = \frac{([M \times g] + \text{down-force}) \times \mu_{max}}{M} = g \times \mu_{max} + \frac{\text{down-force} \times \mu_{max}}{M} , \tag{5}$$

which shows that the acceleration has increased by

$$\frac{\text{down-force} \times \mu_{max}}{M} . \tag{6}$$

Since mass is in the denominator of Eq. (6), it is clear that it is desirable to minimise M to achieve maximum acceleration in all directions. This result remains true, even when a more accurate tyre friction model is used incorporating differences in static and dynamic coefficients of friction. The addition of aerodynamic down-force will usually cause increased drag. This drag force will limit the maximum longitudinal velocity of which the vehicle is capable between corners. This speed will be achieved when the power transmitted by the engine to the ground via the driven wheels is totally absorbed by the drag force produced by the vehicle, Ref. [5]. Consequently a trade-off exists between the additional downward force which is required to maximise both longitudinal and lateral acceleration, and the drag force produced by the addition of this extra down-force which will determine the maximum longitudinal velocity of the vehicle.

1.4 Measuring the influence of aerodynamics on the performance of race cars

Measuring the real-time performance of a race car at speed is essential in allowing the driver and team to maximise their performance on a given circuit layout. Data can be collected in a number of ways to aid in the "set-up" of a race car. The most common of these include: shock position sensors, linear accelerometers, and tyre temperature sensors. Shock position sensors can be used in a number of ways to examine performance of the vehicle; primarily they are used to analyse the performance of the shock absorber in terms of both speed and position. From these data the ride height of the vehicle can be determined, given a known bell crank motion ratio, which can then be used to determine the aerodynamic down-force experienced by the vehicle given a known spring rate and the position of the shock absorber relative to its static position. The use of accelerometers allows both the longitudinal and lateral accelerations of the vehicle to be recorded and displayed in what is often referred to as a 'performance/manoeuvre envelope' or 'G-G' diagram Ref. [6], as shown schematically in Fig. (1).
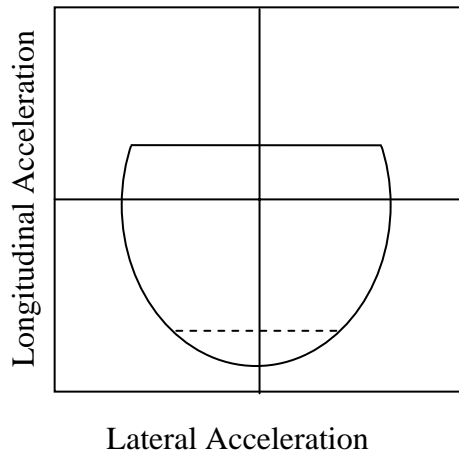
Figure 1: The Performance Envelope

The performance envelope displays both the longitudinal and lateral accelerations recorded by the vehicle while the vehicle is on-track. A two-wheel drive vehicle will produce an optimum 'performance envelope' similar to Fig. (1). These provide an excellent tool for displaying the influence on performance of aerodynamic down-force and drag. The flat line at the top of the envelope is a function of the available engine power and the drag force which limit the amount of longitudinal acceleration in the forward direction. The curve at the bottom of the longitudinal acceleration is a result of the braking power of the vehicle and will shift to the dotted line if the braking power is not adequate [4]. The rest of the curve which connects the braking and longitudinal acceleration is the maximum acceleration achievable during cornering. It is evident that as the forward longitudinal acceleration is increased, the level of cornering performance is reduced; this is a function of the operating characteristics of the tyre.

The 'performance envelope' recorded by a vehicle on a given track does not remain static. It is a dynamic envelope which changes greatly as a result of atmospheric conditions such as ambient and track temperatures as well as humidity, and changes to the set-up of the vehicle. The prime objective is always to expand the performance envelope and hence maximise both the lateral and longitudinal accelerations recorded as these will produce the fastest lap times. The vehicle will always operate within the performance envelope as this dictates the maximum acceleration which the vehicle is capable of in all aspects of performance.

1.5 The current state of aerodynamic design in Formula SAE

A number of aerodynamic design features have been used on vehicles in former Formula SAE competitions. These have included the use of wings and a profiled under-tray. In 2004 the University of Auckland Formula SAE vehicle featured an aerodynamic design unique to the competition which used the shape of both the under-side and top surfaces of the body work to create down-force. In 1990 a "sucker car" (Ref. [7]) was entered in the American competition. The design of this vehicle used sliding skirts to seal the underside of the vehicle and large fans driven by the engine to extract air from under the vehicle and literally suck the car to the track. The advantage of this system is that the down-force is independent of speed, Ref.[8]. The use of fans for any purpose other than cooling was banned the following year. The first winged car with an extremely large single element and bi-plane wings entered in Formula SAE in 2000. In 2004 two entries in the Australasian round of the formula SAE competition used aerodynamic design in the form of wings to produce down-force.

The aerodynamic design of the 2004 University of Auckland entry utilised "ground effect" in its use of two pairs of diffuser tunnels; one pair at the rear and the other in front of the rear wheels. The rear tunnels were angled to ensure that the tunnel could start as far forward as possible while avoiding the chassis rails which protruded from the back of the cockpit area to the back of the engine. The angle of the tunnel was kept constant in order to ensure an increased angle on the inboard part of the tunnels, which would be necessary for the rear part of the tunnel to be horizontal, did not promote separation of the flow from the diffuser surface.

4

2   NUMERICAL MODELLING

The purpose of the CFD analysis was primarily to design the body (including side-pods) and the under-tray of the vehicle prior to carrying out wind tunnel testing.

2.1   Design constraints and considerations

The testing and design freedom involved in the development of the body and under-tray of the car model was heavily restricted by the need to comply with all the relevant sub-systems related to the operation of the vehicle. The most influential of these included the size of the driver's cockpit, the suspension geometry, engine, drive train and their related arterial systems as well as the competition rules. The shape of the cockpit and resultant carbon fibre tub was largely dictated by driver ergonomics. Several wooden mock-ups of the tub were built in order to ensure that each of the prospective drivers could reach all the necessary steering, braking and throttle controls. From these mock-ups critical dimensions were taken and transferred to CAD from which the initial car model was designed.

2.2   Solution methodology and model setup

The CAD models of the car body and under-tray were constructed using ProEngineer Wildfire 2.0, the computational domain was meshed using ICEM CFD mesh builder, and the CFD analysis was carried out using the CFX 5.6 Pre, Solver and Post programs. To get the maximum performance from the available software and hardware, a computational half-model was used (cut along the longitudinal centreline) 13m long, 3m wide, and 2.5m high, giving a blockage of 3.7%, or in terms of the model maximum dimensions: l, w, h: 4.56 x l, 4.69 x w and 3.56 x h. A mesh refinement study was conducted and it was determined, given the computational power available, that the optimal mesh for the study of the body and under-tray consisted of approximately 1.5 million cells. The surface of the model was given an inflated mesh consisting of five layers of inflation with an expansion rate of 1.2 between each layer. The remainder of the mesh was generated using tetrahedral cells with a minimum edge length of 1.4mm and a maximum of 106mm. The software solved the Reynolds Averaged Navier Stokes (RANS) equations, using the Shear-Stress-Transport (SST) turbulence model, Ref. [9], which had been successfully tested and used for research within the Mechanical Engineering Department Ref. [10].

2.3   Effect of exhaust in the outside rear diffuser tunnels

Directing the exhaust gases into rear diffuser tunnels is a means to increase both the mass flow rate and subsequent velocity of the air flow travelling under the vehicle, and as a result to produce a reduction in the pressure under the vehicle (Ref. [11]) and so this was investigated using CFD. The velocity of the exhaust of the vehicle was calculated using an average 'choke' velocity of 300m/s drawn through the mandatory 20mm inlet restrictor to the engine. The mass flow rate through the restrictor was then calculated, and half of this flow was directed to each side of the duel exhaust configuration. The resulting mass flow rate per side was 0.05 kg/s, and gave an exhaust velocity ranging from 65 to 99 m/s for exhaust gas temperatures from 300 to 600°C. In order to avoid the additional complexity and computation time associated with adding buoyancy effects to the computational model, the exhaust temperatures were kept the same as ambient and the area of the exhaust was varied in order to obtain the correct mass flow and momentum rates into the under-tray diffusers. Due to the high velocity of the exhaust gases buoyancy effects were not expected to play a significant role in the diffuser aerodynamics, so ignoring them was justified.

Fig. (2) shows the effect of exhaust gas temperature and mass flow rate on the resulting lift coefficient for the case of a car speed of 15 m/s. As expected, higher mass flow rate and higher exhaust gas speed (from higher exhaust temperature) result in more down-force giving a maximum increase of 35%.
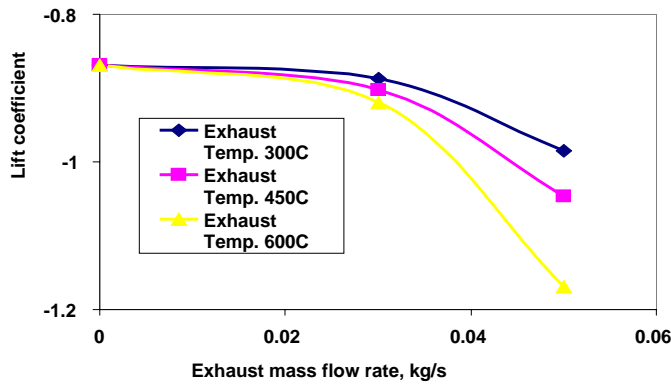

Figure 2: Effect of mass flow rate and gas temperature of exiting exhaust gases into the outside rear diffuser tunnel on the lift coefficient.

Running this same model without the exhaust gave a mass flow rate of 0.0267 kg/s, thus adding the exhaust flow to each tunnel has more than doubled the mass flow rate.

The reduced pressure is evident on the pressure contour plot of the model in Fig. (3) with (right) and without (left) the presence of the exhaust. This area of reduced pressure can be seen by the increase in the area of the green zone in the centre of the model, and near the rear, which is present when the exhaust was included. The presence of the exhaust gases influences as far forward as the entrance to the area under the side pod as shown by the two areas of dark blue.

The reduced pressure in the centre section of the under-tray resulted in a shift of the centre of pressure further forward. The influence of the exhaust caused an increase in down-force on both the front and rear wheels as the mass flow rate of the exhaust was increased for a constant exhaust gas temperature, with a greater increase in the down-force experienced on the front wheels compared to the rear, as shown in Fig. (4).

At a mass flow rate 0.05kg/s the front wheels experienced an 87% increase in down-force over that recorded for a mass flow rate of zero while the rear wheels experienced an increase of 19%. The overall effect of this increase in down-force resulting from the increase in the exhaust mass flow rate for a constant exhaust temperature was to shift the centre of pressure from 0.44m to 0.6m from the rear axle. This is equivalent to a shift in the load distribution between the front and rear wheels of 10% towards the front. This position of the centre of pressure results in 38% of the load being directed into the front wheels and the remaining 62% into the rear. With an exhaust mass flow rate of zero the load split was 28% on the front wheels and 72% on the rear. The addition of
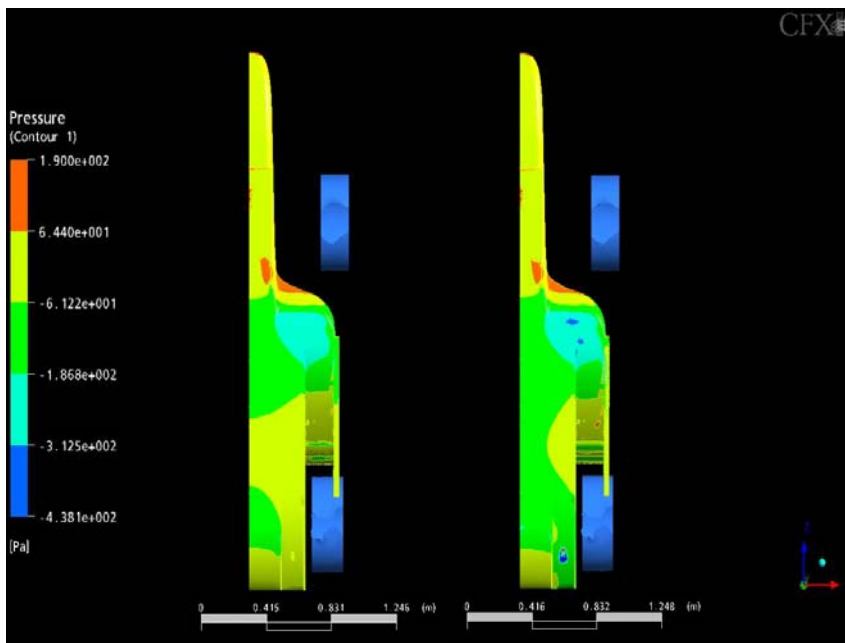

Figure 3: Pressure Contours on the Base of the Undertray without (left) and with (right) the Influence of the Exhaust at a Model Velocity of 15m/s

the exhaust to the outside rear diffuser tunnels produced progressively less influence as the speed of the model was increased. At a model velocity of 30 m/s the addition of the exhaust provided only a 3% increase in down-force.
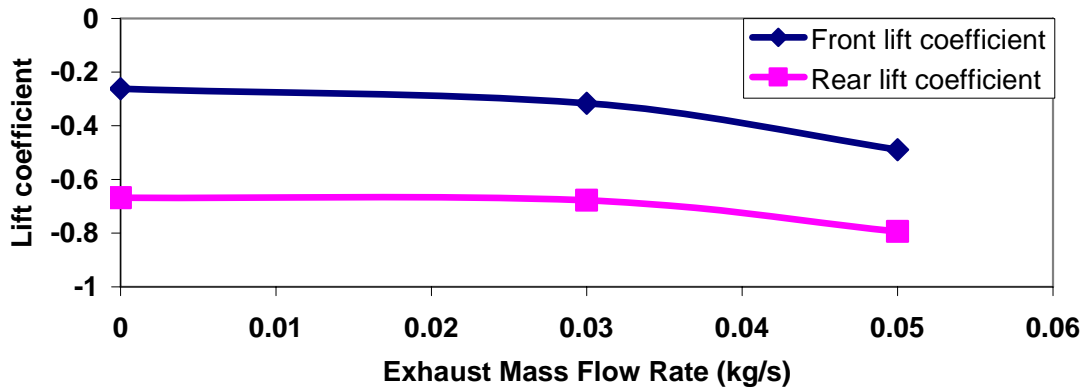

Figure 4: Effect of exhaust mass flow rate on the front and rear lift coefficients

From the analysis of the introduction of the exhaust to the outside rear diffuser tunnel it can be concluded that it will have a larger effect on the ability of the model to generate down-force at lower velocities and will subsequently be at its most influential as the vehicle is exiting a corner or is under heavy engine braking. The influence of the exhaust tapers off as the vehicle velocity increases, and has only a minor effect at velocities in excess of 30m/s.

2.4   Rear wheel tunnel winglets

Two small winglets with 140mm chord lengths were added to the outlet of the rear wheel tunnels in an attempt to "drive" the rear wheel diffuser by providing a reduction in the outlet pressure. It was hoped that this reduction in pressure would draw the higher pressure air out of the tunnel and over the rear wheel.

It was found that the addition of the winglets provided a 7% increase in down-force with no exhaust flow, and an 8% increase with an exhaust mass flow of 0.05 kg/s and a temperature of 600°. The fact that this increase was not equal over the range of exhaust mass flow rates is evidence that the inclusion of the exhaust in the outside rear diffuser tunnels has a positive effect on the under-tray's ability to generate a down-force.
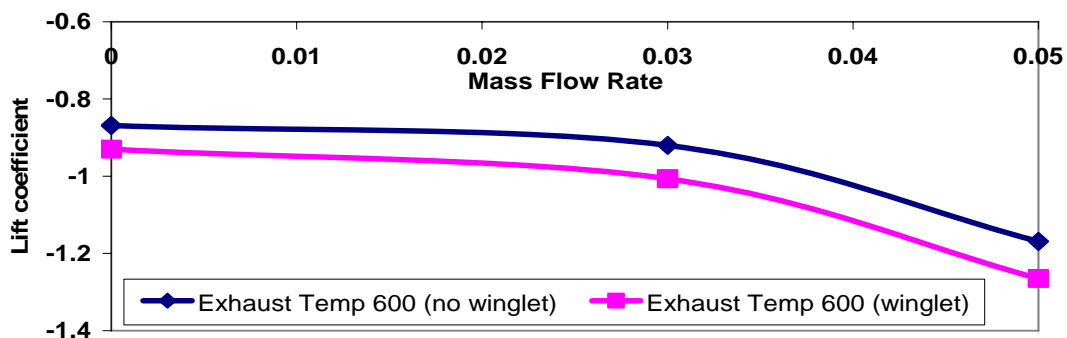

Figure 5: Influence of two rear-wheel-tunnel-winglets on the lift coefficient predicted by the model

3 WIND TUNNEL TESTING

3.1 Rolling road design and setup

Wind tunnel testing of cars with low ground clearance is more accurate when the floor moves at the same speed as the air flow, so that no boundary layer grows. This simulates driving into still air. The 2005 University of Auckland Formula SAE team was fortunate to be able to use a moving belt ground-plane built by Glidepath. The belt was 7 m long and gave a 3m flat length available under the model. The 1.6m wide belt had a top speed of 15 m/s. A vacuum system drawing air at 800 m^3/h through 150 25mm diameter holes drilled into the bed under the belt was used to prevent the belt lifting up towards the model in regions of very low pressure, which it did without the vacuum system. Moving belts are commonly used in Formula 1 wind tunnel testing, Refs. [12-16].
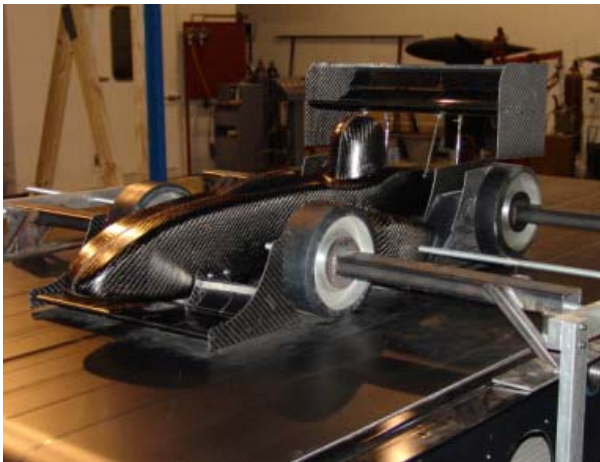
Figure 6: Photograph showing model attached to "sting" above the moving belt groundplane.

All wind tunnel testing conducted using the moving belt was done using a half-scale model made of carbon fibre suspended above the belt by an aluminium 'sting' structure which conveyed all the forces and moments exerted on the model to the six-component balance located in the floor of the test section of the University of Auckland's Twisted Flow Wind Tunnel. The model was tested in an open jet configuration, with a jet that was 3.5m x 3.5m. The car wheels were not attached to the car model, but were positioned accurately and spun by the belt action. This was done to keep the model "live" so that all the aerodynamic forces had to be reacted through the wind tunnel balance. A photograph of the model mounted above the belt is given in Fig. (6).

3.2 The wind tunnel model

The half-scale carbon fibre model of the body was designed using CFD and built from a combination 400g/m^2 carbon fibre cloth and double bias, and resin infused using a vinylester resin. The two halves were then removed from the mould and bonded together using a colloidal silica and vinyl ester bonding agent to create the body of the model. The model was hollow in order to allow the effects of the side pod opening on the flow around and more importantly below the side pod into the ground effect tunnels to be represented as accurately as possible, and it was also lighter than a solid model. It was necessary to have a light model to keep the overall weight within the load capacity of the balance.

The wings of the model were made using pre-impregnated carbon fibre layered in machined aluminium billet moulds. The wings were then fitted to the model and the side pod openings cut and covered with steel gauze. Adjustability was built into the design of the model wings with the angle of attack of each of the elements on the front and rear wings able to be adjusted in 5° increments. The height of the rear wing was also able to be adjusted to match the requirements of the rest of the model. The wing profiles chosen were an adapted version of the Eppler profiles E423 for the main element of the rear wing and the second and third elements for both the front and rear, and the E396 profile for the main element on the front wing. Wing design is a very specialised area in racing car design, Ref. [17]. These pro-

files were chosen primarily as a starting point for the analysis of a wing package. The focus of the present work was on the optimisation of the layout of these adapted profiles. It was initially decided to try to establish a balanced aerodynamic package from a two-element front wing and a three-element rear wing based on the data obtained about the selected profiles, the CFD results from the body and under-tray study, combined with the expected influence of ground effect on the front wing. The wing package was required to provide an aerodynamic load split in the vicinity of 60% on the rear and 40% on the front (which is the static weight split on the vehicle) with a suitable range of adjustability.

3.3   Determination of optimum model location on the moving belt
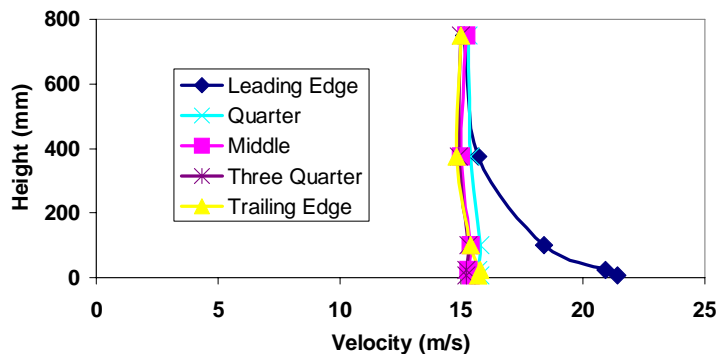
Figure 7: Vertical velocity profiles at various locations along the centreline of the belt

The physical arrangement of the existing wind tunnel meant that positioning the moving belt apparatus had to be a compromise. This is because it was not possible to put the moving belt gear under the wind tunnel floor, as that is where the existing wind tunnel balance is located. Hence the moving belt system had to be positioned on the floor of the test section above the balance near the outlet of the open jet. The performance of various upstream deflectors was investigated in order to attempt to direct the air cleanly over the moving belt. The best arrangement proved to be a sharp trailing edge and-on attached at the downstream end of the moving belt, and surprisingly, with no upstream deflector. Figs. (7,8) show vertical and horizontal velocity profiles respectively above the belt for belt/air speeds of 15 m/s. Based on these re-
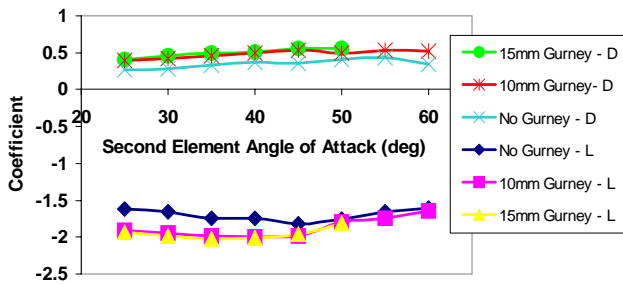
Figure 8: Flow consistency over rolling road moving at 15m/s at a number of heights

sults it was decided to locate the model with its nose at 775mm from the leading edge, as indicated by the vertical line in Fig. (8).

3.4   Independent testing of half-scale wings

The front wings were tested in ground effect equivalent to a 30mm ride height in full-scale above the moving belt, as shown in Fig. (9). The main element of the front wing was tested with an angle of attack of 0° while the secondary elements were tested at 8 different positions ranging from 25° to 60° in 5° increments. These 8 positions were tested first, and then 10mm and 15mm high Gurney flaps were added to the trailing edge of each of the second elements and the 8 different positions tested again. The objective of this testing was to find the best Gurney flap height and angle of the second element. The results are given in Fig. (10). The

front wing produced a maximum lift coefficient of 2.0 with the second element at an angle of attack of 35° with a 15mm high Gurney flap, and had a drag coefficient of 0.5. The benefit of the addition of a Gurney flap to the trailing edge of the secondary elements on front wing began to diminish as the angle of attack was increased above an angle of 35° which was the position of maximum down-force.

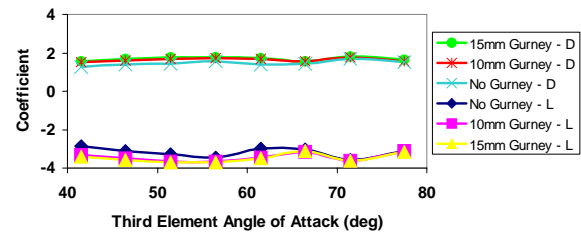The rear wing consisted of one main element combined with second and third elements. The

Figure 9: Independent Front Wing Testing

Figure 10: Lift and drag coefficients for the front wing

Figure 11: Lift and drag coefficients for the rear wing independent of model

main element had an angle of attack of 0° and a chord length of 150mm. The second and third elements both had chord lengths of 75mm. The second element had an angle of attack of 22.5° whereas the third was adjustable between 41.5° and 71.5° in 5° increments. The rear wing was also tested independently in the free-stream (without the moving belt) with and without the 10mm and 15mm Gurney flaps. It can be seen in Fig. (11) that the benefits of the Gurney flaps diminish for angles above 66°, and that there is very little difference in performance of the two Gurney flaps for all angles.

3.5 Half-scale car model testing

The initial testing of the car model complete with front and rear wing was conducted with the wings set to the maximum down-force settings determined from the independent testing described in the previous section. Initial testing was conducted at a number of different velocities between 10 and 15m/s, corresponding to a Reynolds number range between $5x10^5$ - $8x10^5$ (reference length = vehicle length). At 50 km/h, the full-scale Re is about $1.4x10^6$. It was found that over the range of speeds tested, the lift and drag coefficients showed an approximately linear variation with speed, giving increased lift coefficient magnitude and reduced drag coefficient as Re was increased. The slope of these lines enabled the values at full-scale Re to be estimated. For all of the testing conducted on the car model the projected frontal area of the model was used as the reference area for the calculation of aerodynamic coefficients.

The performance of the rear wing was tested on the model by adjusting the angle of the third element. The position of the third element was tested throughout its range of adjustability with three Gurney flap options as discussed in the previous section. It was found that an increase in down-force was accompanied by an increase in drag, as shown in Figs (12,13). The pitching moment coefficient graph had the same shape as the drag graph, indicating the pitching moment was due mainly to drag. Maximum lift, drag and pitching moment were all achieved at an angle of 66° with the 15mm Gurney flap.
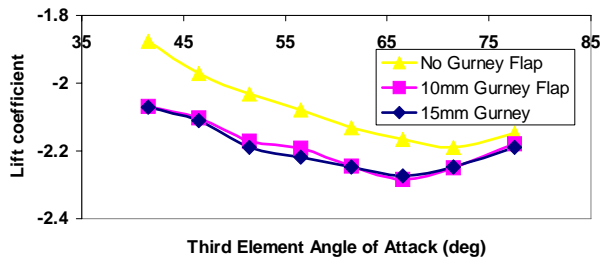
Figure 12: Effect of the addition of a Gurney flap and the angle of attack of the final element on the rear wing on the lift coefficient of the model
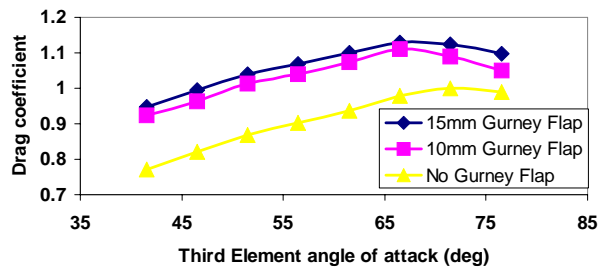

Figure 13: Effect of the addition of a Gurney flap and the angle of attack of the final element on the rear wing on the drag coefficient of the model
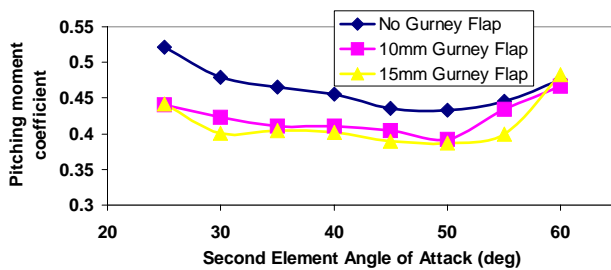

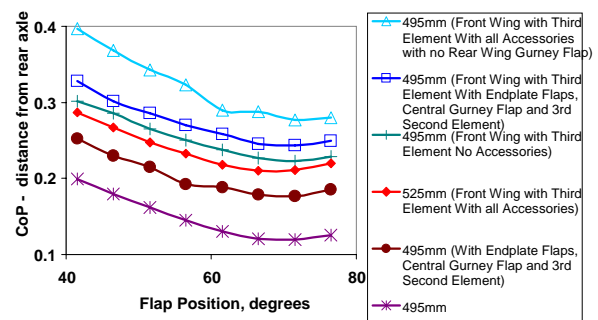Figure 14: Effect of the front wing configuration on the car model pitching moment coefficient.

Figure 15: Rear wing height effect on centre of pressure location.

The two element front wing was tested attached to the car model with and without the two Gurney flaps described previously. The initial testing of the front wing was conducted with the model in the same configuration as had previously been used for the testing of the rear wing with a front ride height of 11mm and a rear ride height of 15mm. The wind tunnel results showed that the effect of angle of attack of the second element as well as the inclusion of the Gurney flaps had only a minor effect on the overall lift coefficient produced by the car model compared to adjustments made to the rear wing. Its effect on pitching moment is shown in Fig. (14). The two Gurney flap options produced a maximum reduction in the overall coefficient of lift of the entire model of less than 0.15 at the position of maximum downforce. This value is less than half the decrease in the coefficient of lift recorded from the addition of the same sized Gurney flaps to the rear wing. The effect of altering the arrangement of the front wing on the overall aerodynamics of the model is significantly more complicated than changes to the rear wing. This is because the wake from the front wing affects both the quality and the quantity of the air flow reaching the two inlets to the under tray under the side pods.

3.6   Centre of pressure position

The effect of the rear wing height and front wing accessories on the location of the centre of pressure are presented in Fig. (15). The aerodynamic appendages enable the centre of pressure to be moved substantially, and give the designer considerable freedom to optimise the design.

11

3.7   Other tests

The effect of vehicle pitch angle was investigated by testing a number of different ride height configurations on the front and rear axle lines of the model. It was found that for the small range of angles tested (corresponding to a change in front ride height of 10mm which is a large fraction of the total suspension movement allowed in the design) the change in down-force with pitch angle was fairly small. A nose-down attitude increased the down-force, which will lead to increased down-force under heavy braking, and vice versa.

Tests at yaw angles up to 20° showed that both the down-force and drag reduced with yaw angle, but the side-force increased, and caused a yaw moment tending to rotate the model inline with the flow. This is generally considered a more stable condition than a yaw coefficient of opposite sign, and was a good result.

4   ON-TRACK EVALUATION OF THE AERODYNAMIC FEATURES

4.1   Data logger setup and recorded data

Data were recorded from the 2006 University of Auckland Formula SAE race car using a MOTEC ADL2 advanced data logger. The data received by the ADL2 which is most useful for the analysis of the performance of the aerodynamic package are those relating the position of the shock absorbers, longitudinal and lateral accelerations recorded by the vehicle, as well as engine parameters such as throttle position, RPM and coolant temperature. The position of the four shock absorbers was determined through the use of four linear potentiometers each of which were individually mounted to the four KONI 2812 shock absorbers. These linear potentiometers mounted on the shock absorbers were used to determine the aerodynamic load placed on each of the four corners of the vehicle (once the suspension noise and load transfer resulting from longitudinal and lateral accelerations were removed). This analysis requires a known centre of gravity, and shock absorber to wheel motion ratio. Two of the three available axes from the accelerometer were utilised to determine the braking, acceleration and cornering performance of the vehicle. These are of particular importance in removing the effect of squat and dive of the vehicle under acceleration or braking in order to isolate the influence of the aerodynamic load on the position of the shock absorber.

4.2   On-track validation of the wind tunnel testing programme

Shock absorber positions were collected at 250 Hz during four acceleration runs during the 2006 Formula Student Germany competition at Hockenheim in order to ascertain the relationship between velocity squared and down-force. As the track was particularly bumpy in places only data recorded from a smooth straight section in the middle of the run were used. After the data received from the shock absorbers were filtered, the influence of squat on the vehicle due to longitudinal acceleration was removed from the data. The resulting loads on the front and rear suspensions were then calculated and plotted against the velocity of the vehicle squared, and gave a linear relationship. This vertical load was converted to a lift coefficient and gave an overall value for the vehicle of -2.1. This value for the full-scale vehicle is only slightly less in magnitude than the value obtained from wind tunnel testing the half-scale model which gave a lift coefficient of -2.22 for the same aerodynamic configuration. This is very good agreement considering the difficulties in measurement in both the wind tunnel and full-scale. It was also evident from the acceleration runs that the location of the centre of pressure was slightly further forward on the vehicle for this configuration than was determined in the wind tunnel. In full-scale a lift coefficient of -0.57 was recorded for the front of

the vehicle whereas the value predicted from wind tunnel testing was -0.52, which again is good agreement.

The difference in lift coefficient and the location of the centre of pressure between the wind tunnel prediction and full-scale measurement could be due to the fact that there was no roll hoop above the driver's helmet in the wind tunnel model. The roll hoop wake could cause a reduction in the performance of the rear wing. This lost efficiency would result in a loss in down-force which would result in a shift of the centre of pressure further forward. Inaccuracies in manufacture, such as the slot spacing between elements on the front and rear wings, as well as possible errors in the estimate of the motion ratio between the shock absorber and the wheel could also contribute to differences between the wind tunnel predictions and the on-track measurements.

4.3 Competition analysis

From measurements of the lateral G-force and vehicle speed made during three laps of the Hockenheim Endurance circuit the track map in Fig. (16) was generated. The fastest lap recorded by the vehicle on the endurance track was on lap three and produced a maximum velocity of 89km/h with a minimum of 22km/h and an average over the entire lap of 50km/h.
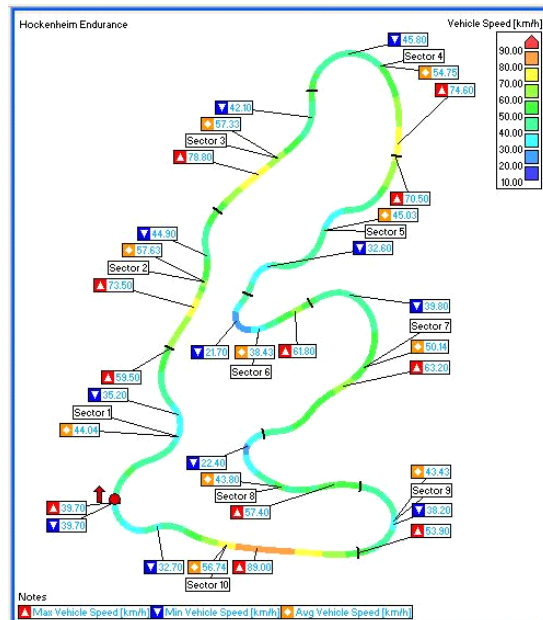

Figure 16: Endurance Event Track Map Displaying Vehicle Speed

Fig. (16) also presents the velocity of the vehicle over the entire track length, which has been split into 10 sectors with the fastest, slowest and average velocities recorded by the vehicle on this lap displayed in each. From this map it is evident that the fastest corner was in sector 4 with a minimum speed of 46km/h while the slowest speed was recorded in sector 8 with a cornering speed of 23km/h.
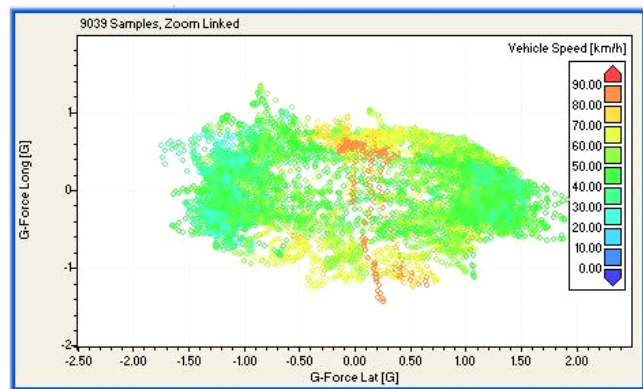

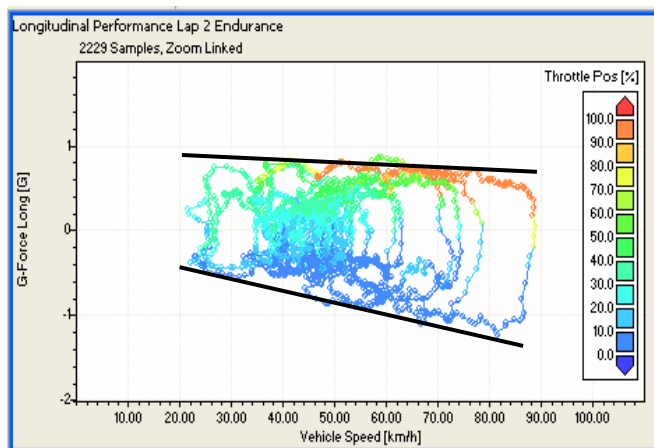Figure 17: Longitudinal G-force Vs. lateral G-force for the fastest recorded lap

Figure 18: Longitudinal performance of the vehicle on the fastest lap

13

The influence of the aerodynamic appendages on the vehicle can be determined from the fastest lap of the track by analysing the recorded G-forces around the circuit. Fig. (17) displays the lateral and longitudinal G-forces recorded by the vehicle during the fastest lap. During this event the front wing was run without the third element and with the second element at an angle of attack of 30° which was less than the optimal of 40° due to concerns related to the efficiency of the engine cooling system.

From these we can see that as the velocity increases so does the G-force with which the vehicle can decelerate. This is clear in the elongation of the diagram with deceleration rates in excess of -1.3G recorded. It is also evident that the majority of cornering took place between 40 and 50km/h. The concentration of data points recorded in the region of both 0.8G longitudinal and 0.8G lateral accelerations at the higher velocities indicates the increased traction experienced on corner exits resulting from aerodynamic down-force.

Fig. (18) shows the G-force as a function of vehicle speed. Two black trend lines have been added to emphasise the effect of speed on longitudinal acceleration, and throttle position has been added to distinguish between braking and acceleration zones. The influence of the drag force and rolling resistance of the vehicle is evident in the reduced ability of the vehicle to accelerate as its velocity is increased. From the top trend line it can be seen that the vehicle is able to accelerate at approximately 0.8G at 24km/h, which reduces to 0.7G at 82km/h. This reduction in acceleration is due to drag forces absorbing more engine power at greater speeds, leaving less available for acceleration. From the bottom trend line it can be seen that as the speed of the vehicle increases the deceleration rate which can be achieved increases substantially. At a velocity of 24km/h the vehicle can decelerate at -0.5G while at 82km/h it can decelerate at -1.3G. The net difference in deceleration is 0.8G, of which 0.1G can be attributed to the drag force and rolling resistance increase between these velocities so approximately 0.7G can be attributed to the increase in aerodynamic down-force produced by the vehicle. Thus the reduction in positive acceleration from the increased aerodynamic drag is substantially less than the gain made in the deceleration.
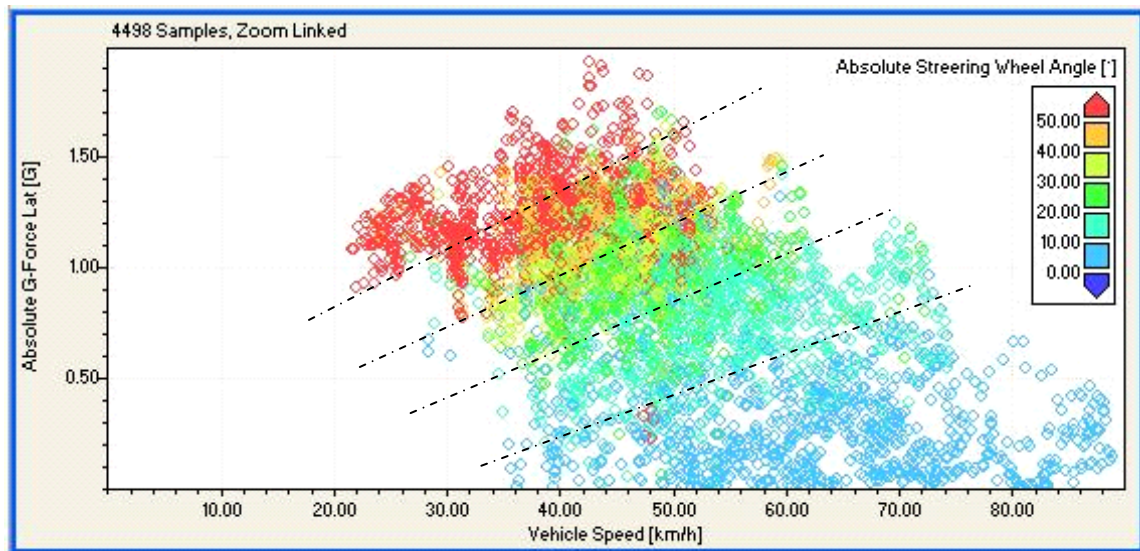

Figure 19: Lateral performance of the vehicle on the two flying laps completed in the endurance event

In Fig.(19) the absolute value of the lateral acceleration recorded by the vehicle is compared with the velocity of the vehicle during the two flying laps completed in the endurance event. The dotted lines have been added in order to emphasise the areas of common steering

angle. It is clear that the majority of the cornering has taken place between 35 and 60km/h. It is also evident that for a constant steering angle input the lateral acceleration achieved by the vehicle increases with speed. As the only influence on the contact of the vehicle with the road which changes with increased velocity is the aerodynamic force, it can be deduced that the aerodynamic treatment of the vehicle is causing this phenomenon.

5   CONCLUSIONS

The objective of designing and testing an aerodynamic package for a Formula SAE race car which maximised the creation of performance enhancing down-force while maintaining a level of drag which would not severely restrict the top speed of the vehicle in the competition was achieved.

From the CFD analysis of the vehicle it was established that a lift coefficient of -0.9 could be obtained from an under-tray design consisting of three rear diffuser tunnels, and one either side in front of the rear wheels.

The addition of the exhaust gas into each of the outside rear diffuser tunnels through a 20mm diameter pipe produced a 35% increase in the amount of down-force produced by the model.

The addition of two winglets of 140mm chord lengths to the trailing edge of the diffuser tunnels ahead of the rear wheel produced an 8% increase in down-force with the exhaust present in the rear diffuser tunnels and a 7% increase without the presence of the exhaust.

Measurements of the air velocity above the rolling road showed that at the centre of the belt the velocity varied by less than 1% from the belt velocity over a height of 750mm from the surface of the belt.

The velocity varied by no more than 2% over a length of 1750mm above the belt when the trailing edge splitter was attached to the downstream end of the unit.

The suction system under the belt was successful in preventing the belt from lifting underneath the model, a phenomenon which was seen to occur without its use.

The wind tunnel testing of a half-scale vehicle model on the rolling road facility determined that a coefficient of lift of -2.4 was able to be obtained with the inclusion of a front and rear wing to the undertray and body designed using the CFD programs.

The three element front and rear wing configurations were able to be adjusted to give a weight split ranging from 43% on the front wheels and 57% on the rear to 33% on the front and 67% on the rear, with a rear wing height of 495mm above the belt.

The car model drag coefficient was able to be adjusted between 0.9 and 1.1.

For the aerodynamic configuration used in the acceleration event at the 2006 Formula Student Germany Competition the vehicle produced 6% less down-force than was predicted from wind tunnel testing the half-scale model. This proved that the wind tunnel with the rolling road facility was a viable means by which to design and test the aerodynamic performance of a Formula SAE race car.

During the endurance event the aerodynamic appendages were seen to be responsible for a significant increase in the performance of the vehicle under braking while the drag force had only a minimal effect on the top speed which was achievable by the vehicle.

The aerodynamic package was seen to provide a significant increase in the cornering speed which was achieved by the vehicle for a given steering angle input.

ACKNOWLEDGEMENTS

Unit who assisted with the wind tunnel testing, financial support from Ipenz, and support from Glidepath and other sponsors who assisted the Formula SAE team.

REFERENCES

[1] S. McBeath. *Competition Car Downforce: A Practical Guide*. Haynes Publishing, Sparkford, Nr Yeovil, Somerset, 2001.

[2] J. Katz. *Race Car Aerodynamics: Designing for Speed*. Bentley Publishers, Cambridge, MA 02138 USA, 1995.

[3] A.R. Hammond. *Development of a rolling road wind tunnel research facility for the aerodynamic design of a Formula SAE race car*. Master of Engineering Thesis, Department of Mechanical Engineering, University of Auckland, New Zealand, 2006.

[4] Wright, P. (2001). *Formula 1 Technology*, SAE International, Warrendale, Pa, USA.

[5] McBeath, S. (2001). *Competition Car Downforce: A Practical Guide*, Haynes Publishing, Sparkford, Nr Yeovil, Somerset.

[6] Katz, J. (1995). *Race Car Aerodynamics: Designing for Speed*, Bentley Publishers, Cambridge, MA 02138 USA.

[7] Wordley, S. (2003). "Seeking an Aerodynamic Edge in Formula SAE." Auto Engineer.

[8] Milliken, W. F., and Milliken, D. L. (1995). *Race Car Vehicle Dynamics*, SAE International, Warrendale, Pa, USA.

[9] ANSYS Incorporated, 2005, Innovative Turbulence Modelling: SST Model in ANSYS CFX, USA

[10] Eisdell Moore, W.P. (2004), Numerical Modelling of a Series of Parametric Spinnakers, ME Thesis, University of Auckland, New Zealand

[11] Cooper, K. R., Syms, J., and Sovran, G. "Selecting Automotive Diffusers to Maximise Underbody Downforce." *2000 SAE World Congress*, Detroit, Michigan.

[12] Stollery, J. L., and Burns, W. K. "Forces on Bodies in the Presence of the Ground." *The First Symposium on Road Vehicle Aerodynamics*, The City University, London.

[13] George, A. R. (1981). "Aerodynamic Effects of Shape, Camber, Pitch and Ground Proximity on Idealized Ground-Vehicle Bodies." *Journel of Fluids Engineering*, 103.

[14] Treymayne, D. (2004). *Formula 1 Design*, Haynes North America, Newbury Park, California.

[15] G.Borello, S.Ferro, S.Limone, G.Ferro, P.Bergamini, and F.B.Quagliotti. (1999). "The Role of the Moving Ground for Automotive Wind Tunnel Testing on Race Cars."

[16] Dimitriou, I., and Garry, K. P. "Use of Narrow Belt for Moving Ground Simulation and its Effects on the Aerodynamic Forces Generated on a Formula-1 Car." *2002 SAE Motorsports Engineering Conference and Exihition*, Indianapolis.

[17] Katz, J. "High Lift Wing Design for Race-Car Applications." *Aerotech '95*, Los Angles, California.